Multilayer network switching rate predicts brain performance

Mangor Pedersen[a,1], Andrew Zalesky[b], Amir Omidvarnia[a], and Graeme D. Jackson[a,c]

[a]The Florey Institute of Neuroscience and Mental Health, The University of Melbourne, Melbourne, VIC 3010, Australia; [b]Department of Psychiatry, Melbourne Neuropsychiatry Centre, The University of Melbourne, Melbourne, VIC 3010, Australia; and [c]Department of Neurology, Austin Health, Heidelberg, VIC 3084, Australia

Edited by Olaf Sporns, Indiana University, Bloomington, IN, and accepted by Editorial Board Member Michael S. Gazzaniga November 15, 2018 (received for review August 29, 2018)

Large-scale brain dynamics are characterized by repeating spatiotemporal connectivity patterns that reflect a range of putative different brain states that underlie the dynamic repertoire of brain functions. The role of transition between brain networks is poorly understood, and whether switching between these states is important for behavior has been little studied. Our aim was to model switching between functional brain networks using multilayer network methods and test for associations between model parameters and behavioral measures. We calculated time-resolved fMRI connectivity in 1,003 healthy human adults from the Human Connectome Project. The time-resolved fMRI connectivity data were used to generate a spatiotemporal multilayer modularity model enabling us to quantify network switching, which we define as the rate at which each brain region transits between different networks. We found (*i*) an inverse relationship between network switching and connectivity dynamics, where the latter was defined in terms of time-resolved fMRI connections with variance in time that significantly exceeded phase-randomized surrogate data; (*ii*) brain connectivity was lower during intervals of network switching; (*iii*) brain areas with frequent network switching had greater temporal complexity; (*iv*) brain areas with high network switching were located in association cortices; and (*v*) using cross-validated elastic net regression, network switching predicted intersubject variation in working memory performance, planning/reasoning, and amount of sleep. Our findings shed light on the importance of brain dynamics predicting task performance and amount of sleep. The ability to switch between network configurations thus appears to be a fundamental feature of optimal brain function.

multilayer networks | switching | dynamic functional connectivity | fMRI | brain performance

Functional MRI (fMRI) has significantly enhanced our knowledge about human brain function (1–3), especially in recent years when it has been used to quantify the brain as a complex functional network (4, 5). Although fMRI-based network analyses have led to several new insights into the spatial and temporal nature of large-scale brain network activity (6, 7), many early fMRI network studies treat spatial and temporal information as separate entities, assuming that brain regions are not interconnected across time and space.

Multilayer network analysis (8, 9) is a novel graph-theoretic model of networks where nodes are connected across time and space. Multilayer networks can be decomposed into modules that span time and space using a multilayer modularity algorithm (10) that estimates the spatiotemporal segregation of nodes forming a subset of nonoverlapping modules or networks. This approach has a major advantage over other time-resolved fMRI connectivity methods as it also provides a "temporal link" or connectivity between adjacent time points. In other words, the multilayer modularity model allows us to track and quantify temporal changes of each node and also when they switch between different module or network assignments (11). Network switching is defined as the rate at which a brain region transitions between different functional networks. Note that this measure has previously been called "node flexibility," as proposed by Bassett and others (11, 12); however, we prefer the term "node switching" (13). Despite multilayer modularity being a relatively new technique, a series of studies suggest that network switching is associated with learning of simple motor tasks (12), attention (14), executive function (15), fatigue (16), and depression (17). These studies suggest that multilayer modularity has an underlying neurobiological basis; however, it remains unknown whether network switching is correlated with the dynamics, or variance, of fMRI connectivity time series, and whether network switching occurs during time periods of high or low network connectivity and complexity. It is important to enhance our understanding of switching and dynamics of fMRI connectivity to reconcile how state changes and switching of networks (topological analysis) may relate to statistical dynamics theory (signal analysis). In an attempt to address these nontrivial questions and gaps in the literature, we investigate network switching in a multilayer modularity model using time-resolved fMRI connectivity data from 1,003 healthy adults provided by the Human Connectome Project (18). We hypothesize that fMRI-based network switching and connectivity dynamics are intrinsically correlated. Given that network switching is likely to be a potentially "strenuous" and metabolically costly event for

Significance

The human brain comprises multiple distinct and highly complex networks responsible for specific functions. Most of our current understanding about functional brain networks comes from studies treating the brain as a static entity, and the spatiotemporal configuration of brain networks remains poorly understood. Using a multilayer network model, we show that brain regions, particularly the lateral frontal and parietal brain areas, transit between different network configurations at a high rate (i.e., have high network switching). This network switching rate predicts performance of higher-order cognitive functions including working memory, planning, and reasoning. In other words, efficient brain network switching appears to be an important aspect of optimal brain function.

Author contributions: M.P., A.Z., A.O., and G.D.J. designed research; M.P., A.Z., A.O., and G.D.J. performed research; M.P. and A.O. analyzed data; and M.P., A.Z., A.O., and G.D.J. wrote the paper.

The authors declare no conflict of interest.

This article is a PNAS Direct Submission. O.S. is a guest editor invited by the Editorial Board.

Data deposition: Brain maps and analysis code used in this study are available at https://github.com/omidvarnia/Dynamic_brain_connectivity_analysis.

[1]To whom correspondence should be addressed. Email: mangor.pedersen@florey.edu.au.

This article contains supporting information online at www.pnas.org/lookup/suppl/doi:10.1073/pnas.1814785115/-/DCSupplemental.

Published online December 13, 2018.

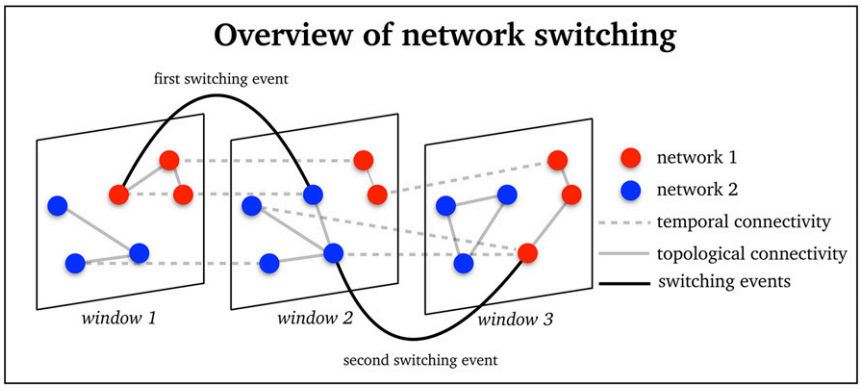

Fig. 1. An overview of network switching within a multilayer modularity network with six nodes and three time windows (window 1, window 2, and window 3) and two modularity partitions (red = network 1; blue = network 2). This example shows two switching events exemplified when node changes between red and blue colors between time points (solid black line between time points). Solid gray lines correspond to within-layer, or topological, connectivity. Dashed gray lines correspond to between layer, or temporal, connectivity.

the brain, we also hypothesize that network switching is associated with changes in fMRI complexity and connectivity. Finally, we hypothesize that network switching is correlated with cognitively demanding behavioral tasks.

Results

Time-resolved fMRI connectivity was estimated with correlation-based sliding-window analysis (19) from $N = 25$ brain nodes (derived from an independent components analysis across all subjects; *SI Appendix*, Fig. S1) and 4,800 time points (~1 h of data concatenating 4 × 14.4-min sessions of fMRI data). We used a window length of 100 s (139 time points). Each window was shifted 0.72 s (one time point) across the whole scan, resulting in a total of 4,661 time windows (W). We then formed a 3D matrix of correlation coefficients of size $N \times N \times W$, composed of 2D $N \times N$ matrices for every time window W. These time-resolved fMRI connectivity data were used as an input to the multilayer modularity model, which was an iterative Louvain community detection algorithm with uniform ordinal temporal coupling between adjacent time points (10). The temporal coupling strength of this model is governed by its parameter ω, whereas the topological resolution of modules is governed by its parameter γ. Low/high ω provides weak/strong temporal coupling between adjacent time points, whereas low/high γ gives few/many spatial modules. The most commonly used parameters in this multilayer modularity algorithm are $\omega = \gamma = 1$. However, to ensure that our results are not affected by a specific spatial and temporal parameter, we calculated multilayer modularity across a range of parameter sets including $\gamma = [0.9, 1, 1.1]$; $\omega = [0.5, 0.75, 1]$, previously found to have strong spatiotemporal modularity (11). For each pair of parameters (ω, γ) the multilayer modularity model was a 2D array of size $N \times W$ containing integer values defining spatiotemporal nodal network assignments. We then calculated nodal network switching as the proportion of layers (time windows) in which a node's network assignment changes (see Fig. 1 for an overview).

Nodes That Switch Networks More Often Fluctuate Less Strongly. First, we assessed whether network switching was related to dynamic connectivity. A connection was deemed dynamic if the SD of its time-resolved functional connectivity was significantly greater than the SD of time-resolved functional connectivity measured in 500 phase-randomized surrogates (20). Connections that did not significantly differ from this surrogate data were consistent with the null hypothesis of a process that was stationary and approximately Gaussian. These connections could still change over time, but more randomly than connections deemed to be dynamic. It is important to remark that the core definition of connectivity dynamics is still under debate (21), and failure to reject the above null hypothesis does not imply that a connection is necessarily static in time.

An uncorrected P value was assigned to the SD value of each fMRI sliding-window connection corresponding to its relative rank compared with the 500 randomized surrogates. This is a one-tailed test that considers whether a connection has stronger, but not weaker, variance than the surrogate data. For example, an fMRI connection will have an uncorrected P value of 0.002 if it has a greater SD value than 499 of the 500 randomized surrogates (calculated as 1 − *rank*/total number of variables, where *rank* = 500 out of 501 total variables). Statistical significance of connectivity dynamics was then determined using a false discovery rate (22) correction with threshold of $q = 0.05$, over all uncorrected P values. To reduce dynamic connectivity information from the level of connections ($[N(N-1)]/2) = 300$) to nodes ($N = 25$), we calculated the binary sum of all significant dynamic connections associated with each node. This resulted in a nodal degree metric quantifying the number of dynamic connections associated with each node.

We found that network switching was inversely correlated with fMRI-based connectivity dynamics. Averaged over all 25 brain nodes, Spearman's correlation between network switching and dynamic connectivity ranged between $\rho = -0.49$ and -0.52, across all ω and γ parameters (Fig. 2*A*, ω and $\gamma = 1$ shown). Across over all 1,003 individuals, Spearman's correlation between network switching and dynamic connectivity ranged between $\rho = -0.51$ and -0.55, across all ω and γ parameters (Fig. 2*B*, ω and $\gamma = 1$ shown). We also replicated this finding in two additional analyses where we increased the spatial resolution while down-sampling the temporal resolution by decreasing the overlap between sliding windows ($N = 50$ and $W = 2{,}330$, where each window was shifted in two time-point increments; $N = 100$ and $W = 1{,}165$ where each window was shifted in four time-point increments; *SI Appendix*, Fig. S2). Temporal resolution was down-sampled to ensure computational tractability.

In line with our prior hypothesis, topological switching and connectional dynamics of networks are (inversely) correlated. Next, we aimed to test whether the switching brain is associated with changes in overall global network connectivity, compared with the nonswitching brain. To this end, we calculated the average correlation coefficient of each sliding-window correlation matrix corresponding to time windows when brain regions switch between networks versus time windows when brain regions do not switch between networks. Given that variation in ω and γ had a negligible impact, we henceforth only consider ω and $\gamma = 1$.

Switching Is Frequent When Global Network Connectivity Is Low. The absolute average sliding-window correlation coefficient of all possible pairwise correlations between nodes was significantly

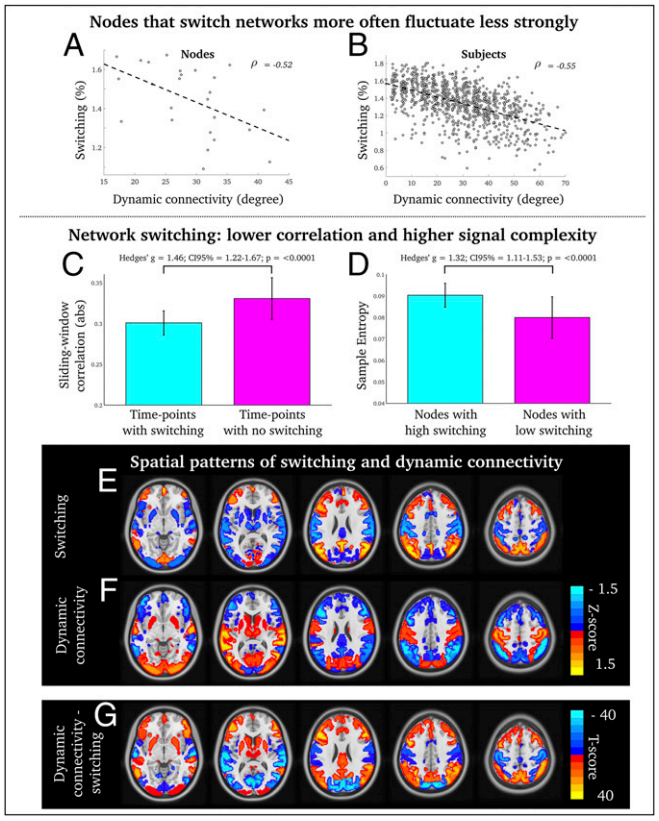

Fig. 2. Scatterplot between network switching and connectivity dynamics. (*A*) Each data point denotes a single node, averaged across all subjects. (*B*) Each data point denotes a single subject, averaged across all nodes. (*C*) During time windows with network switching (cyan color), nodes display significantly lower absolute sliding-window correlations than time windows with no switching (magenta color). (*D*) Average sample entropy in the five nodes with most network switching (cyan color) was significantly higher than the five brain nodes with lowest network switching (magenta color). (*E*) Network switching was high in association cortices and low in primary cortices. (*F*) Dynamic connectivity was high in primary cortices and low in association cortices. (*G*) Paired *t* test difference between the 25 nodes in *E* and *F*. Data for all 25 brain nodes were normalized into z-scores so ensure both connectivity dynamics and switching values were scaled equally and appropriate for univariate *t* test analysis. Network switching is the rate at which a brain region transits between different networks (in percent); dynamic connectivity is the number of connections with significantly stronger fluctuations.

lower during time windows when nodes switch between networks (i.e., between two neighboring layers when the switch occurred), compared with time windows when nodes do not switch between networks (Hedges' g effect size = 1.46, 95th percentile confidence interval = 1.22–1.67, df = 2004, $P < 0.0001$; Fig. 2*C*). Note that we calculated absolute correlation values to avoid positive and negative correlation values cancelling out, resulting in a global network connectivity value close to zero. This result suggests that network switching occurs during periods of low global network connectivity. Given that this analysis was conducted in the topological domain, we next wanted to elucidate whether temporal complexity was also affected by network switching. To this end, we calculated entropy (signal complexity) of brain nodes that switch networks most frequently versus brain nodes that switch networks least frequently.

Association Between Signal Complexity and Switching. We found significantly higher sample entropy (23) (parameter values were $M = 2$, $r = 0.2$ times the SD of fMRI connectivity signals) values of sliding-window correlation time series in the five brain regions with highest rate of network switching (on a group level these brain regions were superior parietal lobule, precuneus, left frontoparietal lobe and right frontoparietal lobe, and right intraparietal sulcus), compared with the five brain regions with lowest rate of network switching (on a group level these brain regions were secondary visual cortex, superior temporal lobe, primary motor cortex, and left cerebellum and right cerebellum) (Hedges' g effect size = 1.32, 95th percentile confidence interval = 1.11–1.53, df = 2,004, $P \leq 0.0001$; Fig. 2*D*). This finding suggests that network switching is associated with temporally complex fMRI connectivity signals.

Our results suggest that (*i*) switching and dynamic connectivity are negatively correlated, (*ii*) switching time windows have lower correlations in the topological domain, and (*iii*) frequently switching nodes have greater complexity in the temporal domain. Following this, we next sought to localize which cortical and subcortical regions switch the most.

Switching Is Most Frequent in Association Cortex. We observed a divergent spatial pattern between network switching and functional dynamics in the case of $N = 25$ nodes. Higher switching was observed in association cortex compared with primary cortex (hot colors in Fig. 2*E*), whereas the converse pattern was evident for connectivity dynamics (hot colors in Fig. 2*F*). Parcellations comprising $N = 50$ and $N = 100$ nodes showed comparable patterns (*SI Appendix*, Fig. S3). In Fig. 2*G*, we report results from a paired *t* test outlining nodal differences between switching and dynamic connectivity. In total, 24 of 25 brain nodes were statistically different between switching and connectivity dynamics after correcting for multiple comparisons (false discovery rate, $q = 0.05$). The only brain region not statistically significant between switching and dynamic connectivity was the secondary visual cortex (node 4 in *SI Appendix*, Fig. S1).

In light of these spatial network findings (Fig. 2 *E* and *F*), we next aimed to confirm that the multilayer modularity algorithm delineated spatial modules conforming to well-known resting-state networks. A module consensus map was generated using a group-averaged agreement matrix that contains probability values [0, 1] denoting the number of times node pairs share the same module divided by the number of possible times two nodes can share the same module. By computing a Louvain clustering algorithm of the group-averaged agreement matrix (see ref. 24 for more details about consensus partitioning of modularity data), we obtained five modules common to all subjects including (*i*) default mode network, (*ii*) sensory networks, (*iii*) frontoparietal network, (*iv*) dorsal attention network, and (*v*) ventral attention network. The first three networks have a strong spatial overlap, whereas the last two networks have a moderate spatial overlap, with resting-state networks delineated using alternative methods of Yeo et al. (25) (*SI Appendix*, Fig. S4).

We also calculated average network switching within our five modules and confirmed that association cortices (default mode, frontoparietal and attention networks) showed significantly higher switching rates, compared with sensory cortices (*SI Appendix*, Fig. S5).

Relationship Between Switching and Behavior. Finally, we aimed to test whether switching predicted interindividual variation in behavior and task performance. Given that the Human Connectome Project offers a wealth of behavioral information (26), we wanted to use a data-driven regression approach without any prior bias. To this end, we included 50 behavioral variables comprising behavioral domains such as cognition (working memory, attention, executive functioning, planning, reasoning, and gambling), social functioning, personality traits, physical function, and sleep. Although we used a data-driven regression approach, we hypothesized that the subset of tasks important for higher-order or frontal lobe function would be most important for efficient brain network switching. These cognitive tasks include

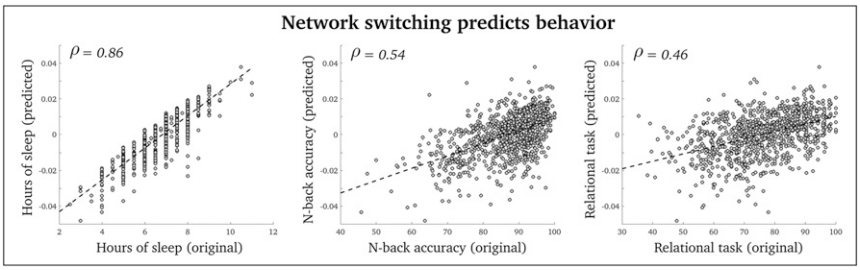

Fig. 3. Scatterplots between elastic net predicted and rescaled behavioral variables (*y* axes) and original values (*x* axes). Each dot is a single subject, and dashed lines denote the best linear fit between predicted and original values.

(*i*) the Flanker task (cognitive inhibition), (*ii*) card-sorting task (cognitive flexibility), (*iii*) processing speed (general cognitive ability), (*iv*) N-back task (working memory), and (*v*) relational task (planning and reasoning).

We used elastic net regression (27) to test whether any of the 50 behavioral domains (independent variables) predicted whole-brain averaged network switching (dependent variable). Elastic net regression is well suited to data-driven regression analysis as it provides a sparse output by removing all behavioral data deemed to be unrelated to network switching. Elastic net is governed a regularization parameter λ that alters the sparsity and variability of the regression model. The regularization parameter was determined with 10-fold cross-validation (28). The minimum mean square error (0.028) was achieved with a regularization parameter $\lambda = 0.023$ (*SI Appendix*, Fig. S6). At this value, behavioral data accounted for ∼3% of the total variance of fMRI network switching data ($r^2 = 0.029$, defined as 1 − [residual sum of squares/total sum of squares] of the regression model). This r^2 value was significantly higher than expected due to chance ($P < 0.001$, compared with r^2 estimates from 500 randomly generated elastic net regressions).

The elastic net regression result at λ of 0.023 showed that 3 of 50 behavioral domains were weakly, but significantly, related to network switching (note that elastic net regression β values were zero for all other 47 measures): *i*) number of hours of sleep the night before the MRI scan (Spearman's correlation between switching and hours of sleep was $\rho = 0.14$, $P < 0.0001$; elastic net regression β was 0.071; the Spearman's correlation between original and predicted data was $\rho = 0.86$; Fig. 3, *Left*)—as hypothesized, higher-order functions were also correlated with switching; *ii*) accuracy of N-back task using the average accuracy score from the 0- and 2-back task, important for working memory (Spearman's correlation between switching and N-back task was $\rho = 0.11$, $P < 0.0001$; elastic net regression β was 0.036; the Spearman's correlation between original and predicted data was $\rho = 0.54$; Fig. 3, *Middle*); and *iii*) relational task involved in planning and reasoning (Spearman's correlation between switching and relational task was $\rho = 0.11$, $P < 0.0001$; elastic net regression β was 0.017; the Spearman's correlation between original and predicted data was $\rho = 0.46$; Fig. 3, *Right*).

Discussion

By leveraging the information-rich brain imaging dataset (approximately 1-h fMRI recordings from 1,003 subjects) provided by the Human Connectome Project (18), we found that the frequency of nodal switching is inversely related to the number of significant dynamic connections (Fig. 2 *A* and *B*), with most prominent network switching in association cortices (Fig. 2*E*). Although it is likely that connections of high switching nodes in association cortex (e.g., bilateral frontal and parietal cortex) also exhibit dynamic activity, our results suggest their variability, as measured with SD, is indistinguishable from phase-randomized surrogate data. We also found that brain nodes switch between networks during time windows with low global network connectivity (Fig. 2*C*), and high-switching nodes were more "temporally complex"—estimated with sample entropy—compared with low-switching nodes (Fig. 2*D*). Switching is known to increase in systems with high entropy or information load (29). We consequently hypothesize that our observed relationship between brain network switching and high entropy/low global network connectivity may be related to increased information load imposed on specific brain regions, especially those located within the association cortex (e.g., bilateral fontal and parietal cortex) known to integrate information between a range of different networks (30).

Network switching also predicted intersubject variation in behavior, using data-driven elastic net regression (Fig. 3). Even though we included a range of behavioral variables including personality traits, physical performance, emotion, and well-being, behaviors that tap into association cortex function were predicted by network switching, including working memory and planning/reasoning (31). We noted a resemblance between our spatial network switching map displayed in Fig. 2*D* and previous task-based fMRI studies of working memory tasks (32), with prominent bilateral frontal and parietal cortices important for higher-order cognitive functions. This warrants investigation of the hypothesis that network switching can predict severity of psychiatric and neurological diseases with pronounced dysfunction of higher-order cognition, such as schizophrenia and epilepsy.

Notably, network switching predicted the amount of sleep that participants had the night before the MRI scan. As all participants were instructed to keep their eyes open during the whole scan, falling asleep in the scanner cannot explain this finding. Sleep impacts on the same domains of brain performance as seen in this study (33), and findings by Betzel et al. (16) also suggest that fatigue may be an important "driver" for network switching. Taken together, this suggests that the impact of sleep deprivation on cognitive performance may be mediated through its effect on brain network switching.

The computational complexity of multilayer network analyses was a limitation of our study, as high spatial and/or temporal resolution of multilayer networks results in very large networks as they are connected in both time and space ($[(N \times W)\ (N \times W)] \approx 10^{10}$ data points per subjects in this study). Given that we needed to include many time windows (here, 4,800 time windows) to statistically detect fMRI dynamic connectivity—this was previously demonstrated by Hindriks et al. (34) and further validated in this study as seen in *SI Appendix*, Fig. S7—we needed to keep the spatial resolution of fMRI data rather coarse (25 brain nodes were used in our main analysis). Although we replicated our original results when increasing the spatial resolution and decreasing the temporal resolution of fMRI networks (*SI Appendix*, Figs. S2 and S3), development of more efficient computational methods for multilayer network modularity detection in the future may mitigate the need for temporal down-sampling.

It is worth noting that the main limitation of only having 25 network nodes is the so-called resolution limit of modularity algorithms. This means that at some point there are an insufficient number of nodes that can converge into segregated and nonoverlapping modules. The resolution limit did not appear to be a problem in the current study as nodes were readily subdivided into well-known "resting-state networks" across subjects associated with relatively high modularity scores ($Q = \sim 0.6$) serving as a quality function of the obtained multilayer modularity partitions (*SI Appendix*, Fig. S4).

Materials and Methods

Subjects, fMRI Data, and Processing. We used resting-state fMRI data from 1,003 healthy adults from the Human Connectome Project, accessible via https://www.humanconnectome.org/study/hcp-young-adult/article/release-s1200-extensively-processed-rfmri-data (18, 35) (female subjects = 534/1,003; male subjects = 469/1,003), and Institutional Review Board approval was considered unnecessary for the current study. fMRI recon r177+r227 data were used and subjects were between ages of 22 and 35 y. fMRI parameters included echo time = 33.1 ms, field of view = 208×180 mm^2, number of slices = 72, voxel size = 2 mm^3, and flip angle = 52°. We used four fMRI scans for each subject (14.4 min per scans where subjects were instructed to keep their eyes open). At a repetition time of 0.72 s there were 1,200 time points in each scan; we concatenated all four scans into continuous fMRI time series comprising 4,800 time points.

The fMRI data of each subject was preprocessed by the Human Connectome Project team with echo planar imaging gradient distortion correction, motion correction, field bias correction, spatial transformation and normalization into a common Montreal Neurological Institute space (36), and artifact removal using independent component analysis FIX (37). A group-level independent component analysis was used to define the 25 brain nodes of interest, common across all subjects. We additionally filtered the fMRI data between frequencies of 0.01 and 0.1 Hz.

fMRI Correlation-Based Sliding-Windows Analysis. We used a Pearson's correlation-based sliding-window analysis to estimate time-resolved fMRI connectivity. Pearson's correlation coefficient of two resting-state fMRI time series (38, 39) $X[t]$ and $Y[t]$ is written as

$$r = \frac{\sum_{t=1}^{T}(X[t]-\bar{X})(Y[t]-\bar{Y})}{\sqrt{\sum_{t=1}^{T}(X[t]-\bar{X})^2}\sqrt{\sum_{t=1}^{T}(Y[t]-\bar{Y})^2}},$$

where $\bar{X}$ and $\bar{Y}$ are the sample means and r have a numerical range between −1 (anticorrelation) and 1 (correlation). Here, the pairwise correlation coefficient between 25 brain regions of interest was calculated based on a fixed window length consisting of 139 fMRI time points (100 s), which satisfies the $1/f_0$ wavelength criterion for a minimum cutoff frequency of 0.01 Hz (19, 40, 41). Windows were shifted with a single time point, resulting in a total number of 4,661 windows. We tapered each correlation-based window with a Hamming function to mitigate edge artifacts of the windows and attenuate potentially noisy signals.

Multilayer Modularity and Network Switching. To quantify spatiotemporal network switching we used an iterative and ordinal Louvain algorithm to track network function over time (10) [implemented with codes from Lucas G. S. Jeub, Marya Bazzi, Inderjit S. Jutla, and Peter J. Mucha, "A generalized Louvain method for community detection implemented in MATLAB," netwiki.amath.unc.edu/GenLouvain/GenLouvain (2011–2016)]. Modularity is quantified by Q ranging from 0 (low network segregation) to 1 (high network segregation). This measure is governed by γ and ω parameters, which determine the strength of topological and temporal connectivity, respectively. Multilayer modularity is written as follows:

$$Q(\gamma,\omega) = \frac{1}{2\mu}\sum_{ijsr}\left[\left(A_{ijs}-\gamma_s\frac{k_{is}k_{js}}{2m_s}\right)\delta(M_{is},M_{js})+\delta(i,j)\cdot\omega_{jrs}\right]\delta(M_{is},M_{jr}).$$

A_{ijs} is the sliding-window correlation matrix between node i and j for time point s, whereas $k_{is}k_{js}/2m_s$ (k = node degree at time point s, m = sum degree of all nodes at time point s) denotes the Newman–Girvan null model of intranetwork connectivity. As this multilayer modularity algorithm only allows positive matrix values, we removed all negative correlations in the sliding-window matrices, A. γ_s is the topological resolution parameter of time point, or layer, s and ω_{jrs} is the temporal coupling parameter for node j between time window r and s. Then, $\delta(M_{is},M_{js})$ and $\delta(M_{is},M_{jr})$ are 1 if nodes belong to in the same module and 0 if they do not belong to the same module (M). This process was, on average, iterated five times before the inherent heuristics of the multilayer modularity algorithm converged. Networks had an average Q-value of 0.59 ± 0.012 SD and an average of three modules per subject (range: two to six modules). The final output of the multilayer modularity algorithm was a 2D array ($N \times W$) with integer values denoting modules with strong within-network connectivity. The switching rate for each node was then estimated as the percentage of time windows when a brain node transitions between different network assignments. As discussed previously, it is a nontrivial issue to select ω and γ parameters and we used a range of parameters including γ = [0.9, 1, 1.1] and ω = [0.5, 0.75, 1]. As shown in *SI Appendix*, Fig. S8, the temporal ω parameter appeared to alter spatiotemporal modularity more than the topological γ parameter. Specifically, lower ω values led to increased network switching. Nodes switched 1.61% of the time for $\omega = 0.5$, 1.55% of the time for $\omega = 0.75$, and 1.48% of the time for $\omega = 1$, at a constant γ-value of 1.

fMRI Dynamic Connectivity. The SD of fMRI sliding-windowed correlation time series between node pairs was here used as a proxy of dynamic connectivity, where high SD indicates greater signal dispersion from mean correlation-based sliding-window time series. To determine whether our obtained SD values of time-resolved fMRI connectivity likely reflect "true dynamics" (meaning that we obtain information from this measure that cannot be obtained in time-averaged, or static, analysis), we compared SD between original and phase-randomized data where fMRI time series were phase shuffled in the Fourier domain while preserving the power spectral magnitude and the correlational nature of the data (20). We obtained 500 phase-randomized signals and used false discovery rate ($q = 0.05$) to reduce probability of type-I errors given that each subject has 300 unique comparisons. In total, 28.9% of node pairs were deemed "dynamic" after correcting for multiple comparisons. To convert the dynamic connectivity data from matrix ($[(N(N-1)/2)] = 300$) to node ($N = 25$) space, we summarized the (binary) number of significant connections for each node, resulting in a degree metric summarizing how dynamic a node is.

Sample Entropy. For each subject, we used sample entropy to estimate the difference in temporal complexity of time-resolved fMRI connectivity signals between five nodes with most network switching and five nodes with least network switching. We used a template length, M, of 2 and a tolerance parameter, r, of 0.2× the SD of the signal (see ref. 23 for more information about sample entropy). In brief, a low sample entropy score suggests that a signal includes structured patterns, whereas a high sample entropy score suggests that the signal is random or unpredictable.

Cross-Validated Elastic Net Regression. We used elastic net to test whether whole-brain averaged network switching predicted 50 behavioral variables across subjects. Elastic net enables data-driven regression analysis by enforcing sparsity of regression output values (i.e., reducing the number of final β regression values). In other words, it provides automatic variable selection by removing all behavioral variables not predicted by network switching.

Given that network switching data and behavioral data had different numerical scales, we normalized all input data, x, which denotes both switching data and the 50 behavioral variables:

$$\bar{x} = \frac{x - \text{mean}(x)}{\max(x) - \min(x)}.$$

This resulted in variables, $\bar{x}$, with values between −1 and 1. The elastic net equation is then written as

$$\hat{\beta}_0,\hat{\beta} = \arg\min_{\beta_0,\beta}\left\{\sum_{i=1}^{n}\left(y_i-\beta_0-\sum_{j=1}^{p}\beta_j X_{ij}\right)^2+\lambda\sum_{j=1}^{p}\left[\frac{1}{2}(1-\alpha)\beta_j^2+\alpha|\beta_j|\right]\right\},$$

where y is a vector of size $1 \times 1{,}003$ containing subject-specific information from whole-brain averaged network switching data and X is a matrix of size $50 \times 1{,}003$ containing subject-specific information from 50 behavioral variables. This is a doubly penalized regression model using both LASSO regression ($\alpha = 1$; an $l-1$ penalty resulting in a sparse but uncorrelated β values) (42) and Ridge regression ($\alpha = 0$; an $l-2$ penalty resulting in a variance-reducing, but nonsparse β values) (43). We set the α value to 0.5 to take advantage of the relative strengths of the two above regression approaches, providing a nonsparse solution with low variance among several correlated independent variables (*SI Appendix*, Fig. S9).

To select a λ threshold, which determines the overall sparsity of the regression model, we calculated elastic net over a range of different λ values

between 0 and 1 with increments of 0.001 (total of 1001 λ values) using 10-fold cross-validation (~900 people were trained and ~100 people were left out for testing, repeated 10 times until all subject have been left out once for training). The "optimal" threshold had lowest mean square error over all possible λs across the 10-folds. We found $\lambda = 0.023$ had the lowest mean square error of 0.028 (*SI Appendix*, Fig. S6).

As reported in the text, our results showed network switching predicted 3 of 50 behavioral variables. We defined prediction as

$$\text{Prediction} = X\beta + \beta_o,$$

where X is the original values of our three behavioral variables and β_o is the intercept of the elastic net regression model.

ACKNOWLEDGMENTS. All fMRI data in this study have been made freely available by the Human Connectome Project, WUMinn Consortium (1U 54MH091657; Principal Investigators David Van Essen and Kamil Ugurbil) funded by the 16 NIH institutes and centers that support the NIH Blueprint for Neuroscience Research, the McDonnell Center for Systems Neuroscience at Washington University, and National Health and Medical Research Council (NHMRC) of Australia Grant APP628952. The Florey Institute of Neuroscience and Mental Health acknowledges the strong support from the Victorian Government and in particular the funding from the Operational Infrastructure Support Grant. We also acknowledge the facilities and the scientific and technical assistance of the National Imaging Facility at the Florey node and The Victorian Biomedical Imaging Capability. G.D.J. is supported by NHMRC Practitioner's Fellowship APP1060312. A.Z. is supported by NHMRC Senior Research Fellowship B (APP1136649).

1. Bandettini PA, Wong EC, Hinks RS, Tikofsky RS, Hyde JS (1992) Time course EPI of human brain function during task activation. *Magn Reson Med* 25:390–397.
2. Kwong KK, et al. (1992) Dynamic magnetic resonance imaging of human brain activity during primary sensory stimulation. *Proc Natl Acad Sci USA* 89:5675–5679.
3. Ogawa S, et al. (1992) Intrinsic signal changes accompanying sensory stimulation: Functional brain mapping with magnetic resonance imaging. *Proc Natl Acad Sci USA* 89:5951–5955.
4. Bullmore E, Sporns O (2009) Complex brain networks: Graph theoretical analysis of structural and functional systems. *Nat Rev Neurosci* 10:186–198.
5. Rubinov M, Sporns O (2010) Complex network measures of brain connectivity: Uses and interpretations. *Neuroimage* 52:1059–1069.
6. Hutchison RM, et al. (2013) Dynamic functional connectivity: Promise, issues, and interpretations. *Neuroimage* 80:360–378.
7. Preti MG, Bolton TA, Van De Ville D (2017) The dynamic functional connectome: State-of-the-art and perspectives. *Neuroimage* 160:41–54.
8. De Domenico M (2017) Multilayer modeling and analysis of human brain networks. *Gigascience* 6:1–8.
9. Muldoon SF, Bassett DS (2016) Network and multilayer network approaches to understanding human brain dynamics. *Philos Sci* 83:710–720.
10. Mucha PJ, Richardson T, Macon K, Porter MA, Onnela J-P (2010) Community structure in time-dependent, multiscale, and multiplex networks. *Science* 328:876–878.
11. Bassett DS, et al. (2013) Robust detection of dynamic community structure in networks. *Chaos* 23:013142.
12. Bassett DS, et al. (2011) Dynamic reconfiguration of human brain networks during learning. *Proc Natl Acad Sci USA* 108:7641–7646.
13. Telesford QK, et al. (2017) Cohesive network reconfiguration accompanies extended training. *Hum Brain Mapp* 38:4744–4759.
14. Shine JM, Koyejo O, Poldrack RA (2016) Temporal metastates are associated with differential patterns of time-resolved connectivity, network topology, and attention. *Proc Natl Acad Sci USA* 113:9888–9891.
15. Braun U, et al. (2015) Dynamic reconfiguration of frontal brain networks during executive cognition in humans. *Proc Natl Acad Sci USA* 112:11678–11683.
16. Betzel RF, Satterthwaite TD, Gold JI, Bassett DS (2017) Positive affect, surprise, and fatigue are correlates of network flexibility. *Sci Rep* 7:520.
17. Zheng H, et al. (2018) The dynamic characteristics of the anterior cingulate cortex in resting-state fMRI of patients with depression. *J Affect Disord* 227:391–397.
18. Van Essen DC, et al.; WU-Minn HCP Consortium (2013) The WU-Minn human Connectome Project: An overview. *Neuroimage* 80:62–79.
19. Zalesky A, Breakspear M (2015) Towards a statistical test for functional connectivity dynamics. *Neuroimage* 114:466–470.
20. Prichard D, Theiler J (1994) Generating surrogate data for time series with several simultaneously measured variables. *Phys Rev Lett* 73:951–954.
21. Liégeois R, Laumann TO, Snyder AZ, Zhou J, Yeo BTT (2017) Interpreting temporal fluctuations in resting-state functional connectivity MRI. *Neuroimage* 163:437–455.
22. Benjamini Y, Hochberg Y (1995) Controlling the false discovery rate: A practical and powerful approach to multiple testing. *J R Stat Soc Series B* 57:289–300.
23. Richman JS, Moorman JR (2000) Physiological time-series analysis using approximate entropy and sample entropy. *Am J Physiol Heart Circ Physiol* 278:H2039–H2049.
24. Lancichinetti A, Fortunato S (2012) Consensus clustering in complex networks. *Sci Rep* 2:336.
25. Yeo BTT, et al. (2011) The organization of the human cerebral cortex estimated by intrinsic functional connectivity. *J Neurophysiol* 106:1125–1165.
26. Barch DM, et al.; WU-Minn HCP Consortium (2013) Function in the human connectome: Task-fMRI and individual differences in behavior. *Neuroimage* 80:169–189.
27. Zou H, Hastie T (2005) Regularization and variable selection via the elastic net. *J R Stat Soc Series B Stat Methodol* 67:301–320.
28. Lachenbruch PA, Mickey MR (1968) Estimation of error rates in discriminant analysis. *Technometrics* 10:1–11.
29. Amigó JM, Kloeden PE, Giménez Á (2013) Entropy increase in switching systems. *Entropy* 15:2363–2383.
30. van den Heuvel MP, Sporns O (2011) Rich-club organization of the human connectome. *J Neurosci* 31:15775–15786.
31. Courtney SM, Petit L, Maisog JM, Ungerleider LG, Haxby JV (1998) An area specialized for spatial working memory in human frontal cortex. *Science* 279:1347–1351.
32. Wager TD, Smith EE (2003) Neuroimaging studies of working memory: A meta-analysis. *Cogn Affect Behav Neurosci* 3:255–274.
33. Alhola P, Polo-Kantola P (2007) Sleep deprivation: Impact on cognitive performance. *Neuropsychiatr Dis Treat* 3:553–567.
34. Hindriks R, et al. (2016) Can sliding-window correlations reveal dynamic functional connectivity in resting-state fMRI? *Neuroimage* 127:242–256.
35. Van Essen DC, et al.; WU-Minn HCP Consortium (2012) The Human Connectome Project: A data acquisition perspective. *Neuroimage* 62:2222–2231.
36. Glasser MF, et al.; WU-Minn HCP Consortium (2013) The minimal preprocessing pipelines for the Human Connectome Project. *Neuroimage* 80:105–124.
37. Salimi-Khorshidi G, et al. (2014) Automatic denoising of functional MRI data: Combining independent component analysis and hierarchical fusion of classifiers. *Neuroimage* 90:449–468.
38. Keilholz SD, Magnuson ME, Pan W-J, Willis M, Thompson GJ (2013) Dynamic properties of functional connectivity in the rodent. *Brain Connect* 3:31–40.
39. Zalesky A, Fornito A, Cocchi L, Gollo LL, Breakspear M (2014) Time-resolved resting-state brain networks. *Proc Natl Acad Sci USA* 111:10341–10346.
40. Leonardi N, Van De Ville D (2015) On spurious and real fluctuations of dynamic functional connectivity during rest. *Neuroimage* 104:430–436.
41. Pedersen M, Omidvarnia A, Zalesky A, Jackson GD (2018) On the relationship between instantaneous phase synchrony and correlation-based sliding windows for time-resolved fMRI connectivity analysis. *Neuroimage* 181:85–94.
42. Tibshirani R (1996) Regression shrinkage and selection via the lasso. *J R Stat Soc Series B* 58:267–288.
43. Hoerl AE, Kennard RW (1970) Ridge regression: Biased estimation for nonorthogonal problems. *Technometrics* 12:55–67.